

Journal Pre-proofs

Unravelling the Structural Changes of Phospholipid Membranes in Presence of Graphene Oxide

Priya Mandal, Gourav Bhattacharya, Arpan Bhattacharyya, Susanta S. Roy, Sajal K. Ghosh

PII: S0169-4332(20)33009-9
DOI: <https://doi.org/10.1016/j.apsusc.2020.148252>
Reference: APSUSC 148252

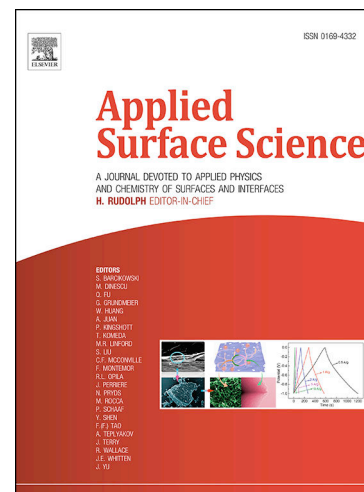
To appear in: *Applied Surface Science*

Received Date: 21 August 2020
Revised Date: 13 October 2020
Accepted Date: 21 October 2020

Please cite this article as: P. Mandal, G. Bhattacharya, A. Bhattacharyya, S.S. Roy, S.K. Ghosh, Unravelling the Structural Changes of Phospholipid Membranes in Presence of Graphene Oxide, *Applied Surface Science* (2020), doi: <https://doi.org/10.1016/j.apsusc.2020.148252>

This is a PDF file of an article that has undergone enhancements after acceptance, such as the addition of a cover page and metadata, and formatting for readability, but it is not yet the definitive version of record. This version will undergo additional copyediting, typesetting and review before it is published in its final form, but we are providing this version to give early visibility of the article. Please note that, during the production process, errors may be discovered which could affect the content, and all legal disclaimers that apply to the journal pertain.

© 2020 Published by Elsevier B.V.



Unravelling the Structural Changes of Phospholipid Membranes in Presence of Graphene Oxide

Priya Mandal^a, Gourav Bhattacharya^{a§}, Arpan Bhattacharyya^b, Susanta S. Roy^a

and Sajal K. Ghosh^{a}*

^aDepartment of Physics, School of Natural Sciences, Shiv Nadar University, NH-91, Tehsil Dadri, G. B. Nagar, Uttar Pradesh 201314, India

^bS. N. Bose National Centre for Basic Sciences, Block JD, Sector-III, Salt Lake, Kolkata 700106, India

*Corresponding author: Tel: +91-120-7170100, Extn. 410, sajal.ghosh@snu.edu.in

Present Address

[§]Nanotechnology and Integrated Bioengineering Centre, School of Engineering, University of Ulster, Newtownabbey, BT370QB Northern Ireland, UK.

Abstract

Graphene-based nano-technology is the future of biomedical devices including biosensors and, hence, it is essential to unravel the interaction of graphene oxide (GO) with cellular membrane. Here, the structural reorganization of lipid molecules, which are the building blocks of a cellular membrane, has been demonstrated in presence of GO flakes. The membrane is mimicked by forming a stack of lipid bilayers of zwitterionic phospholipid 1,2-dipalmitoyl-sn-glycero-3-phosphocholine (DPPC) and its structures have been probed by x-ray reflectivity and grazing incidence x-ray diffraction techniques. Lipid-GO composites have exhibited two sets of lamellar diffraction peaks illustrating GO-rich micro-domains in the matrix of phospholipid bilayers (GO-poor phase). In these domains, the GO flakes are observed to penetrate into hydrophobic core of the bilayer altering the thickness along with the overall electron density profile of the lipid layer. The GO-poor bilayer is closely related to the phase formed by pristine

lipid molecules. The lattice parameters of a body-centred rectangular unit cell formed by chains of saturated phospholipid are found to be modified in the presence of GO with a significant effect on molecular tilt. The structural description of GO-membrane interaction may pave the way of discerning the physical behaviour of the composites.

Keywords: Graphene oxide, lipid membrane, x-ray scattering, electron density profile, lipid chain configuration.

1. Introduction

Graphene oxide (GO) holds an atomically thin 2D structure with a range of oxygen functionalities such as carboxyl groups on the edges and hydroxyl and epoxies on the basal plane [1, 2]. Presence of these functional groups makes the GO molecules dispersed in water facilitating their applications in cellular imaging [3, 4], drug-delivery [5], bio-sensing [6] and antibacterial activities [7]. The useful and efficient applications of these molecules in the field require an in-depth knowledge of self-assembly of GO in lipid membrane. This membrane is important in this context as it mimics a cellular membrane which is primarily composed of a lipid bilayer enclosing the intracellular compartments. This cellular membrane is the first target of any foreign molecules interacting with a cell [8].

Using molecular dynamic (MD) simulation, it has been revealed that a stack of few graphene layers can diffuse into the membrane interior resulting in a thicker bilayer [9]. This study, however, left the room to experimentally realize the findings. There are reported efforts to stabilize phospholipid membranes on a graphene surface for developing biosensors and biocatalysis [10]. As functionalized graphene molecules including GO have a much broader scope of applications, researchers today have shown immense interests in the complex of GO and lipid membrane [11]. These molecules have reported being toxic to microorganism as well as human cell line [12, 13] which has been explained by the disruption effects of the molecule on the cellular membrane [14]. Through simulation, Chen et al. have concluded that the GO

molecules can penetrate into the membrane and pull out lipids to form a pore [15]. However, suitable experimental verification of such findings still remains a challenge. In their surface analytical technique of quartz crystal microbalance, Frost et al. have monitored the self-assembly of the complex predicting the adsorption of GO-flakes onto the lipid membrane [16]. Such adsorption has also been reported by Li et al. using lipid monolayers formed at air-water interface [17]. These studies have predicted that positively charged lipid head group is suitable to interact with GO having negatively charged $-COO^-$ groups on its edges. There are studies claiming that there is no complex formation between GO and the zwitterionic phospholipids [17, 18]. On the contrary, some other groups have quantified the interaction between GO molecules and the neutral phospholipids [19, 20]. These contradictions have to be resolved for further advancement of the field.

Even though there are multiple approaches to predict the self-assembled structures of GO-lipid complexes, there is no concrete x-ray scattering study in the field to unambiguously provide the quantitative description of the structure in molecular level. In a recent study, the interlayer separation in multilamellar vesicles formed by (reduced-)GO and a single chain synthetic cationic surfactant was calculated from the position of the diffraction peaks [21]. In the present study, advanced x-ray scattering techniques, namely x-ray reflectivity (XRR) and grazing incidence x-ray diffraction (GIXD), have been employed to study the complex in a multilayered lipid system formed on a solid substrate. The study aims to explore the interaction between a zwitterionic phospholipid and GO flakes from the structural aspect, particularly addressing the question, how GO flakes modify the out-of-plane and in-plane organizations of lipid molecules in a membrane. In the process, the location of the GO molecules in and around the membrane has been quantified.

2. Materials and methods

2.1. Materials

Neutrally charged lipid 1, 2-dipalmitoyl-sn-glycero-3-phosphocholine (DPPC) was purchased from Avanti Polar Lipids (Alabaster, AL) in powder form and used without further purification. Spectroscopic grade methanol and chloroform were purchased from Sigma Aldrich (USA), whereas H_2SO_4 , KMnO_4 and H_2O_2 were purchased from Fisher Scientific. De-ionized (DI) (Milli-Q, Millipore) water with resistivity $\sim 18 \text{ M}\Omega\text{cm}$ and $\text{pH} \sim 7$ was used throughout the experiment.

2.2. Methods

2.2.1. Synthesis and characterization of GO nanoflakes: Graphene oxide (GO) nano-flakes were synthesized from pure graphite powder following the modified Hummer's method [22]. X-ray photoelectron spectroscopy (XPS) data have shown ~ 30 atomic percentage of oxygen in the synthesized GO flakes. The details of the synthesis methodology have been provided in supporting materials. The synthesized flakes were measured to be 0.7 - 1.0 nm thick with a lateral size of 180 - 200 nm as characterized by field emission scanning electron microscope (FESEM) and atomic force microscope (AFM) (Figure S1(a), (b) and (c)). The x-ray diffraction peak at 11.03° (Figure S1 (d)) corresponding to a length scale of 7.83 \AA suggests the synthesis of GO-flakes which was confirmed by Fourier transform infrared (FTIR) (Figure S1 (e)) and UV-visible (Figure S1(f)), spectroscopic data.

2.2.2. Lipid multilayer sample preparation: To prepare lipid multilayers, polished silicon (Si) substrates (100) were cut into $8 \times 15 \text{ mm}^2$ pieces and cleaned ultrasonically using 15 min cycles of methanol and DI water, respectively followed by drying in a gentle flow of N_2 . To make hydrophilic, the substrates were exposed to UV radiation for 20 minutes at 25°C . Chloroform was used to prepare a lipid solution to a final concentration of 5 mg/ml and an

aqueous solution of GO was taken to achieve a certain wt. % of GO in the mixture. Then the mixture was vortexed to get a uniform solution. 60 μL of this solution was deposited uniformly onto a cleaned Si substrate and left for 2 hours in a fume hood for slow evaporation of the solvent. Then the samples were placed in a vacuum chamber for 24 hours to remove the traces of the solvent and incubated at 50 $^{\circ}\text{C}$ for 36 hours in a chamber with controlled relative humidity (RH) maintained by a saturated salt solution [23]. A set of samples with pure lipid and different wt. % of GO was prepared and sealed in a custom-designed sample cell for x-ray scattering measurements. Multiple samples at the same RH and temperature with varying concentrations of GO in the lipid multilayer in same sample cell ensured almost identical thermodynamic conditions for the given set of samples. RH of 85%, 95% and 98% inside the sample cell were achieved by using saturated salt solutions of KCl, KNO_3 and K_2SO_4 , respectively [24].

2.2.3. Surface sensitive x-ray scattering: To characterize the structural details of the membrane-GO complexes, two surface-sensitive x-ray scattering techniques have been employed, namely the x-ray reflectivity (XRR) and grazing incidence x-ray diffraction (GIXD). In XRR study, scattered data were collected from the multilayer samples following the specular reflectivity conditions (Figure 1). The measurements were carried out at the Indian Beamline (BL-18B), Photon Factory, Tsukuba, Japan with a monochromatized x-ray source of photons with a wavelength $\sim 0.775 \text{ \AA}$ and a beam dimension of $\sim 0.5 \text{ mm (V)} \times 1 \text{ mm (H)}$. For XRR, three multilayer samples with varying GO concentrations were placed in a closed sample cell at a given RH. The scattered photons were collected using a scintillation detector as a function of incident angle in the range of 0 to 4.5° with a step size of 0.005° . The reflectivity profile was obtained by subtracting the background followed by normalization with respect to the incident beam flux (monitor counts). The data were recorded at three different humidity to

achieve slightly varying lamellar spacing intending to obtain the phase factors after applying the swelling method [25].

GIXD technique is very useful to determine the in-plane structure of a flat sample. The glancing angles were kept constant ($\theta_i = 0.12^\circ$ and 0.30°) while the data were collected using a Pilatus (Dectris, Switzerland) detector (Figure 1). The sample conditions were same as XRR measurements except for the sample to detector distance was altered to 180 mm to capture the expected diffraction pattern. The typical exposure time was 300 sec for each scan. GIXSGUI software was used to extract the diffraction data from the 2D spectrum [26].

2.2.4. Atomic force microscopy (AFM): The local morphology of the lipid multilayer samples was acquired using an atomic force microscope (AFM, XE7, Park System). An NCHR tip of resonance frequency 330 kHz and force constant 40 N/m was used in non-contact mode. A particular sample was scanned at multiple locations with a scan rate of 0.4 Hz. Numerous samples of same composition were prepared to obtain the statistical behavior of the topography. For all the measurements, scan area was fixed to $20 \mu\text{m} \times 20 \mu\text{m}$ with a resolution of 512×512 pixels.

3. Results and discussions

As reviewed by Pabst et al. [27], lipid multilayer is a well-established system to mimic the cellular membrane as it exhibits a quasicrystal arrangement of lipid bilayers facilitating x-ray and neutron scattering techniques to provide in-depth structural details of the system. Firstly, the out-of-plane diffraction data are utilized to obtain an electron density profile of a bilayer, that reveals the modified structural parameters such as lamellar repeat distance, bilayer thickness etc. in the presence of any foreign molecules in and around the bilayer. Secondly, the in-plane organization of lipid molecules can be acquired from the grazing incidence diffraction data which can provide the primitive unit cell parameters, chain tilt etc [28]. A schematic diagram of these techniques has been explained in Figure 1.

3.1. Out-of-plane organization of lipids in membrane:

Figure 2 (a) shows a representative set of XRR patterns obtained from the stacked DPPC lipid bilayers on a hydrophilic Si substrate due to one-dimensional periodicity along the substrate normal. The oriented multilayer stacks of lipid molecules give rise to equidistant Bragg peaks acquired at relative humidity (RH) of 85, 95 and 98%. As a consequence, the inter bilayer separation changes by a few Å while the structure of the individual bilayer remains intact [29-31]. This is the well-known swelling method [32-39] which has been implemented here for phase determination. The method has been described in details elsewhere [40-42]. In brief, the amplitude of the form factor of a bilayer is related to the integrated intensity of Bragg peaks modified by the Lorentz correction factor for oriented lipid multilayers [43]. Due to mirror plane symmetry of the bilayers along the bilayer normal, the phase factors are reduced to ± 1 .

The diffraction data obtained from DPPC multilayers are fitted using a single Gaussian to each Bragg peak to obtain the intensity of the peak utilizing a MATLAB code. The determined phase factors for pure DPPC sample are found to be $[-1, -1, -1, -1, -1, -1]$ as shown in Figure 2(b). Note that the phase factors reported in literature for this lipid system may differ as it highly depends on purity of the lipid and the sample temperature [23]. Using the form factor amplitudes and phase factors, the electron density profile (EDP) along the lipid long axis (z -axis in Figure 1) is obtained in arbitrary unit using equation 1 as given below [44-46],

$$\rho_{relative}(z) = \frac{2}{d} \sum_n v(n) n \sqrt{I_n} \cos\left(\frac{2\pi n z}{d}\right), \quad (1)$$

where, d is the lamellar spacing, $v(n)$ and I_n are the phase factor and integrated intensity of n^{th} order diffraction peak, respectively. The EDP of pure DPPC bilayer is shown in Figure 2(c) exhibiting two maxima of the head-group regions of lipid molecules in two opposing leaflets of a bilayer. As the hydrocarbon chain region has much lower electron density compared to the head group regions, it shows a deep in the middle with a variation from the two head group

regions. The electron density profile presented here is in arbitrary unit as reported in previous publications [47-50]. The main aim of the present work is to track down the position of the GO flakes in the model membrane and corresponding changes in the length and size of various components of the membrane. A relative change in the respective structural components will be sufficient for the purpose. The electron density of a lipid bilayer can also be provided in absolute scale [51-53].

Representative x-ray diffraction profiles of DPPC multilayers collected at fixed RH of 85% in presence of different wt. % of GO are shown in Figure 3. In the inset of the figure, the XRR profile of pure GO flakes sample prepared following the same protocol of lipid multilayers is given that shows no reflectivity peak. The DPPC multilayers data obtained at RH 95% and 98% are given in Figure S2. In presence of GO, there are two distinct sets of equidistant XRR peaks representing coexistence of two lamellar phases with different lamellar repeat distances (*d-spacings*). One of them shown with a green arrow which is similar to the pristine lamellar phase of pure DPPC multilayer in regards to the shape of the respective Bragg peaks. This phase is named as GO-poor phase while the other as GO-rich phase. As is evident from Bragg peaks, shown with pink arrow, this new GO-rich lamellar phase is quite different from that of the pristine DPPC phase. The lamellar repeat distance for pure DPPC multilayer is 54.65 Å at 98% RH. With an increase of GO concentration, the Bragg peaks in both the phases are observed to shift towards lower q_z confirming an increase in the lamellar *d-spacings*. At 15 wt. % of added GO, there is an increase of about 2.5 Å in GO-poor phase. At the same concentration, for GO-rich phase, the increase is about 6 Å. Further, the Bragg peaks are observed to be broadened with a modified intensity in presence of GO suggesting a disordering effect on the lamellar structure [54]. This effect is prominent in GO-rich phase compared to the GO-poor phase. The *d-spacings* of various compositions of the GO-rich and GO-poor phases at different RH are given in Table S1.

For quantitative description of the structural effects of the GO molecules on the lipid bilayer, the XRR data are fitted using equation (1) to obtain the EDP of a bilayer. The profiles of GO-poor and GO-rich phases are obtained following the analysis of phasing as shown in Figure S3. For locating the GO molecules in the bilayer, each of the EDP has been decomposed into multiple components [23, 40, 55]. For pure DPPC and the GO-poor phase of the composite, each head group region of the EDP is fitted with two Gaussians and the methyl group region with one Gaussian superimposed on a constant baseline (B). Hence, there are a total of five Gaussians to accommodate two symmetrically located head groups and a chain in the middle. For GO-rich phase, each chain region was modelled with two Gaussians providing a total of six Gaussians for the best fit. The cumulative general expression of the electron density profile, $\rho(z)$ is given by,

$$\rho(z) = B + \sum_n A_n e^{-\frac{(z-z_n)^2}{2\sigma_n^2}} \quad (2)$$

where $n = 1$ to 5 for GO-poor phase and 1 to 6 for GO-rich phase. Here, the position (z_n) and the width (σ_n) of the Gaussians are important parameters to relate the position and length scale corresponding to the size of head and chain regions of lipids in the membrane. The EDPs and corresponding Gaussian fits are shown in Figure 4 with the fitting parameters tabulated in Table 1. Since the electron density is not in absolute scale, the density values have not been compared to quantify the presence of GO in the membrane. Rather, the changes in the position (z_n) and width (σ_n) (full width at half maxima – FWHM) of respective Gaussian of the head and chain regions have provided the information about the presence of GO in the membrane.

From this analysis, it is found that the pristine DPPC bilayer has a thickness of ~ 43 Å which is very close to the value reported earlier [33, 56]. The corresponding thickness of head group ($\sigma_{Head\ 1}$) and chain region ($\sigma_{Chain\ 1}$) are 6.51 and 5.40 Å, respectively (Table 1). The chain

region is positioned at the middle of the profile ($z_{Chain\ 1} = 0$) placing the two head group regions symmetrically on either side. The general features of EDPs in GO-poor and GO-rich phases are quite different. While in GO-poor phase, the whole profile is smeared out in comparison to pristine DPPC membrane, the GO-rich phase exhibits a pronounced chain region. It shows a modified nature in the middle of the profile at the meeting junction of two methyl groups. To accommodate such profile, it was necessary to take one more Gaussian compared to the GO-poor phase. As shown in Figure 5(a), the size of head group ($\sigma_{Head\ 1}$) for GO-poor phase has an increase of about 7 Å in the presence of 15 wt. % GO compared to the pristine DPPC phase, while the respective change in GO-rich phase is only about 2 Å. Similar trend is also observed in the width of Gaussian related to the second region of the head group ($\sigma_{Head\ 2}$). This second region may be looked as the interface of hydrophilic head and hydrophobic chains. Interestingly, there is no change in the size of the chain ($\sigma_{Chain\ 1}$) in the GO-poor phase compared to the pristine DPPC phase. In contrast, the separation between the positions of two chains ($z_{Chain\ 2} - z_{Chain\ 1}$) in GO-rich phase is higher from that of the size of pristine DPPC chain ($\sigma_{Chain\ 1}$) (Figure 5(b)). Hence, it is readily understood that there is a strong effect of GO in the head group region of the membrane in GO-poor phase while the GO-rich phase shows the prominent effect in the hydrocarbon chain region. In Figure 5(c), the thickness of each bilayer ($d_{HH} = (z_{Head\ 4} - z_{Head\ 1})$) which is the separation between the symmetric positions of two extreme Gaussians of two head groups is shown as a function of added GO into the multilayer of DPPC lipids. The change in d_{HH} for the GO-rich phase is much higher than that of GO-poor phase. At 15 wt. % of GO, Δd_{HH} is ~ 6 Å for GO-rich phase which is almost twice the value of GO-poor phase.

3.2. In-plane organization of lipids in membrane:

From the analysis of XRR data, it is evident that the GO flakes are distributed non-uniformly in the lipid bilayers. As a consequence, there are two different lamellar phases; one having the

flakes mostly in the head group region while the other having them in the chain region. Both the lamellar phases are expected to exhibit an effect in the organization of lipid chains. Such an effect is quantified by the grazing incidence x-ray diffraction study as has been explained in the following section.

As shown in Figure 6(a), the diffraction data of pristine DPPC collected on a 2D detector display two sharp spots in the $q_{xy}q_z$ plane. The sharpness of the peaks decreases drastically in the presence of GO flakes which exhibits a structural reorganization of the chains [57]. The intensity of the peaks is plotted as a function of q_{xy} (Figure 6(b)). Since the crystalline domains of lipid chains are randomly oriented in the x-y plane, the q_x and q_y components cannot be separated and hence the data has been plotted as a function of q_{xy} which is $(q_x^2 + q_y^2)^{\frac{1}{2}}$ [28, 58-60]. In the gel phase, below their chain melting temperature (~ 42 °C), DPPC molecules are known to form in-plane two dimensional crystalline structures [33, 61]. Such crystalline structures provide Bragg peaks depending on the type of the lattice formed by lipid tails. In the present case, the diffraction peaks of all the lipid compositions are fitted with two Lorentzian functions to follow the features of the peaks [62]. As the DPPC molecules make a tilt with respect to the lipid bilayer normal, there are non-zero q_z component and the intensities are plotted as a function of this component of wave vector transfer in Figure 7. However, with 5 wt. % added GO, there is only one non-zero q_z peak, while the 15% GO does not provide any non-zero q_z peak.

The two Bragg peaks of pristine DPPC are observed at $q_{xy} = 1.23 \pm 0.01$ and 1.32 ± 0.01 Å⁻¹ which are indexed as (11) and (02) planes of a centered rectangular lattice with the lattice parameters of 6.02 ± 0.01 and 9.54 ± 0.02 Å. These lattice parameters were calculated from,

$$d_{hk} = \frac{1}{\sqrt{\frac{h^2}{a^2} + \frac{k^2}{b^2}}} \quad (3)$$

where, $d_{hk} = 2\pi/q_{hk}$. The coherence length was calculated from Scherrer formula [63, 64], $L_{xy} = 0.89(\frac{2\pi}{FWHM_{intrinsic}(q_{xy})})$ where the full width at half maxima (FWHM) of a peak is calculated from, $FWHM_{intrinsic}(q_{xy}) = \sqrt{FWHM_{expt}(q_{xy})^2 - FWHM_{reso}(q_{xy})^2}$. $FWHM_{expt}$ is the value obtained from the Lorentzian fit of the respective peak and the $FWHM_{reso}(q_{xy})$ is the instrument resolution (0.005 \AA^{-1}). The lattice constants (a and b), correlation length (L_{xy}) and other structural parameters are summarized in Table 2. For the lipid multilayers, the rectangular lattice has already been reported in their multiple publications by T- Nagle et al. [65-67]. Also, Raghunathan et al. have reported such an organization of DPPC molecules with the parameters comparable to the present study [68]. Note that this lattice can also be explained as a distorted 2D hexagonal lattice with the peaks indexed as [(0,1), (1,0)] and (1, -1), respectively [69]. On adding the GO flakes in the DPPC multilayer, one asymmetric Bragg peak is observed which is fitted, again, with two Lorentzian functions. The q_{11} peak is observed to shift towards the higher value of q_{xy} while the q_{02} peak to a lower value (Figure 6(b)). Correspondingly, the lattice parameter a decreases and b increases, slightly. Most importantly, both the coherence lengths decrease drastically suggesting a disordering effect of GO-flakes on the organization of lipid chains.

As shown in Figure 7, for pristine DPPC, there are two peaks at $q_z = 0.31 \pm 0.01$ and $0.59 \pm 0.01 \text{ \AA}^{-1}$. These two out of plane peaks suggest a molecular tilt towards next-nearest-neighbor (NNN) molecule as described by Kaganer et al. [60]. For such an organization, the tilt angle (τ) is calculated by, $\tan \tau = \frac{q_{nz}}{q_{nxy}}$ where, ' n ' denotes the non-degenerate peaks [70, 71]. The molecular tilt for pure DPPC lipid is calculated here to be $25.80 \pm 0.01^\circ$ which is slightly lower than the reported values of 27.20° [72] and 26.80° [69]. Such a deviation may be related to the different hydrodynamic pressure on the membrane controlled by relative humidity. Further, the interchain interaction may differ depending on the purity of the lipid and the temperature of

the experiment. What is important in the present study is the relative change of the tilt angle in the presence of the GO molecules. With the insertion of 5% GO into DPPC multilayer, a considerable change observed in the position of the Bragg rods providing only one peak at $0.221 \pm 0.019 \text{ \AA}^{-1}$. The two in-plane Bragg peaks ($q_{xy} = 1.24 \pm 0.02$ and $1.30 \pm 0.01 \text{ \AA}^{-1}$, Figure 6(b)) and one out of plane Bragg rod give rise to a molecular tilt towards nearest neighbor (NN) which is calculated by,

$$\tan \tau = \frac{q_{dz}}{\sqrt{q_{dxy}^2 + (q_{nxy}/2)^2}} \quad (4)$$

obtaining a value of tilt angle $10.90 \pm 0.02^\circ$. Here, 'd' denotes the 'degenerate' peak. The transition of NNN to NN tilt of the lipid chain is an interesting observation which is induced by the GO molecules. At higher concentration, there is no peak at non-zero value of q_z suggesting disappearance of tilt in the chain.

As mentioned earlier, GO-poor phase is close to the pristine DPPC lamellar phase with the GO-flakes accumulated near the head group region. Here, the lipid chains may retain their 2D crystalline structure to some extent at low concentration of GO flakes. However, the presence of GO flakes in the head group region will affect the inter-head group interaction modifying the effective head group area which, in turn, is expected to influence the organization of the chains in the hydrophobic core. In case of GO-rich phase, the presence of GO molecules in the hydrophobic interior is expected to randomize the chain organization providing higher conformational entropy and exhibiting no diffraction peak in the GIXD experiment.

3.3. Further discussion

The lipid molecules spontaneously self-assemble into a bilayer so that the hydrocarbon chains of the lipids can avoid interaction with the water molecules [73]. Many of such bilayers form a stack on a hydrophilic surface to form the smectic liquid crystalline phases [74]. For a single component lipid system, such a one-dimensional crystalline structure provides equidistant

peaks in XRR study [75]. However, in case of multicomponent system, because of hydrophobic mismatch in chain length and differences in chain conformations, there have been reports of phase-separated domains of one type of lipids in the matrix of the other [76, 77]. In the present study, the GO flakes are adsorbed on the membrane surface in GO-poor phase, while in GO-rich phase, they are trapped in the hydrophobic chain region. Due to the hydrophobic mismatch, the thicker GO-rich phases would separate out themselves from that of the thinner GO-poor phase. From sharper Bragg peaks of GO-poor phase in the XRR measurements, it can be inferred that this phase is the dominant one occupying major sample volume and providing long-range correlation among the bilayers. Hence, GO-poor phase can be considered to form the matrix in which the domains of GO-rich phase are floating. The phase-separated smaller domains become larger in the process of reducing the line tension at the interface of the GO-rich and GO-poor phases [78]. Such an explanation has been discussed in the context of formation of macro-domains in multicomponent lipid systems [79]. The phase-separated domains of GO-rich phase are visualized in the form of patches in the AFM images as shown in Figure 8. Even in a pure DPPC sample, there are patches of smaller size and height as quantified in the height distribution (Figure 8 (a) and (b)). Here, the patches are originated due to the existence of mosaicity in the sample. The patches become much bigger with a height of about an order of magnitude larger in the presence of GO flakes (Figure 8 (c) and (d)). This huge height difference in the AFM topography of samples in the presence of GO flakes is resulted from the long-range correlation among the domains of GO-rich phase in the individual membranes (across the multilayers and along z-direction in Figure 1). Of course, this height difference is not the difference between the GO-rich and GO-poor domains in only two adjacent bilayers, rather the cumulative differences of multiple bilayers. Such an arrangement of one type of domains in the matrix of other is expected to produce two distinct sets of Bragg peaks in a XRR study which is observed in the present case.

The long-range correlation among the domains across the membrane normal is an effect of restructuring of hydrogen bonding networks in the water molecules attached to the head group region of the membrane. Because of controlled relative humidity, the sandwiched water layer between two opposing bilayers is very thin ($\sim 10 \text{ \AA}$) and hence the water molecules will have more ordered structure compared to that of the bulk [80]. As the electrostatic nature of the head group regions of GO-rich and GO-poor phases are different, the water molecules will bind them differently leading to a dissimilar ordering of the water molecules attached to these two phases. When these two dissimilar water networks meet each other, there will be an epistructural surface tension penalty at the interface [81, 82]. To reduce such energetically unfavorable interfaces, the domains may prefer to align along surface normal (across the lipid multilayers).

Graphene oxide (GO) has both the hydrophilic and hydrophobic parts. While the carboxylic groups at the edges, phenol hydroxyl and epoxide groups at the basal plane provide the hydrophilicity, the hydrophobicity arises due to its intact carbon-carbon sp^2 domains. As described by Wu et al., the interaction between a GO molecule and a zwitterionic lipid membrane having no net charge but a permanent dipole moment is a complex process arising from multiple force components [19]. The negatively charged phosphate group attached to the lipid head may have an electrostatic repulsion with the carboxyl groups attached at the edge of the GO flakes. However, this group at the edge provides an electrostatic attraction with positively charged choline group of the head. This long-range attractive force has been attributed as the driving force of the GO molecules to get adsorbed on the zwitterionic lipid membrane [14, 83]. There is also contribution of short-range hydrogen bonding between the GO and the phosphate group of the lipid heads. Even though this hydrogen bonding interaction is weak, there are numerous carboxyl groups at the edge of the GO flakes, which may

effectively drive the adsorption of GO on the lipid membrane. The hydrophobic interaction arises between the graphitic patches of the flakes and the alkyl chain of the lipid.

Not only a lipid molecule but also other amphiphilic molecules have shown hydrophobic interaction with GO flakes. In their experimental study, Li et al., have reported that the hydrophobic part of the amphiphile pluronic F127 interacts with GO flakes [84]. Therefore, both the hydrophilic and hydrophobic interactions play roles in deciding the self-assembled structures of the GO-lipid complexes. While the hydrophilic head groups of lipids will try to align the flakes lying flat on the lipid layer, the hydrophobic interaction may bring it close to the hydrocarbon chain region. Therefore, the question arises about the factors that decide the final organization of GO flakes in a lipid membrane. The stable structure will be determined by multiple factors, such as, (i) percentage of oxidation of a graphene flake, (ii) the size of the GO flakes and (c) the thermodynamic conditions. If the graphene is highly oxidized, the hydrophilic interaction may overshadow the hydrophobic interaction, thereby providing the GO flakes lying flat on the bilayer. Whereas, the simulation work by Puigpelat et al. [85] with 0-20% oxidized graphene has predicted the insertion of GO in the membrane with very slow kinetics. This is because of the attractive interaction between the hydrophobic region of the flakes and the lipid chains, finally leading to a vertical arrangement of partly oxidized graphene sheets into the hydrophobic core of the membrane in its stable configuration. The simulation work by Chen et al. [15], has established that even for highly oxidized GO flakes, the size decides their location in the membrane. The small size GO flakes ($2.1 \times 2.1 \text{ nm}^2$ – $3.1 \times 4.1 \text{ nm}^2$) were found to pull the lipids out of the membrane to form a pore in a few nanoseconds. However, the large size GO flakes were reported to lay flat in the middle of the membrane. This structure did not change over the time duration of simulation providing the flakes stabilized into the hydrophobic region. The simulation was started with the GO flakes keeping

horizontal in the bilayer and it was hard for the large flakes to rotate in the membrane. Therefore, along with the size of the flakes, the initial thermodynamic conditions of the system also played a role to lead the large flakes to remain in the hydrophobic core of the membrane. To the best of our knowledge, all the simulation works reported in literature with GO flakes are performed with an in-plane size of < 5 nm [15, 85].

In the present study, the GO flakes have the lateral size ranging from 180-200 nm, which is two orders of magnitude larger than the ones reported in simulation works mentioned above. The organization of this large size GO flakes in the membrane would be different from that of small size flakes depending upon the initial anchoring sites of the lipid on the flakes. In the present study, initially, the chloroform solution of sample contains the dispersed lipid molecules as monomers and the GO flakes distributed homogeneously in the solution. Following the electrostatic attraction and hydrogen bonding discussed above, it is likely that hydrophilic regions of many of the flakes may expose to lipid heads and locally form a nano-size GO-lipid complex. Over time of slow evaporation of the solvent spread over the Si-surface, they may self-assemble into the GO-poor phase having the flakes attached to the head group region. As $\sim 30\%$ atoms are oxygen in the synthesized GO flakes, there are numerous carbon-carbon sp^2 domains in the flakes. Hence, there is also a probability that the graphitic patches of the GO flakes come closer to the hydrocarbon chain of the lipids. The initially formed nanostructures of GO flakes decorated with lipid chains attached on both the sides of the flakes may end up with the flakes being around in the hydrophobic region of the membrane. As mentioned above [15], these large flakes, thereafter, may not be able to rotate themselves across the multiple lipid bilayers, and thereby being trapped in the GO-rich phase.

4. Limitations and future prospects

As reported earlier and discussed above, size of the GO flakes has significant role in directing the location of the flakes in a lipid membrane. Even though multiple simulation studies have predicted pore formation by GO flakes, to the best of our knowledge, there is still no unambiguous experimental evidence of such pore in a membrane. It is probably because of the size mismatch between the simulation and the experimental works. An experimental protocol has to be developed to synthesize the flakes of similar dimension used in simulation works. The synergetic experimental and simulation works will be able to shed further lights on the structure of GO-membrane complex. In future, grazing incidence small angle x-ray scattering (GISAXS) experiment may be performed to verify the formation of large dimensional pore in a membrane. For such an experiment, a proper experimental geometry is needed at a synchrotron x-ray source. We also need a better model membrane to obtain good quality data under this advanced experimental arrangement. Although the lipid multilayer samples are considered to be excellent model systems to perform biophysical studies on cellular membrane, it has restricted degrees of freedom. Therefore, a system has to be explored where the inter bilayer spacing is such that the out of plane fluctuations of the membrane as a whole and the in-plane dynamics of lipids in the membrane are not restricted. This is possible in 100% humidity condition where a couple of bilayers may float in bulk water keeping them together by short range van der Waals interaction. Such a system will be more realistic and desist of any metastable state.

Besides understanding the interaction of GO with model membrane and corresponding structural changes in the membrane, the knowledge of present study may help in extending the applications of graphene-based materials. The GO-rich phase explained here, can be used to develop bio-electronic devices as the phospholipid membrane electrically isolate the GO sheets from external stimuli. As described by Mohanty et al. [86], the GO-membrane composite can

be used for developing a single-bacterium biodevice, label-free DNA sensor and polyelectrolyte chemical transistor. Present study may help in designing such devices. Further, the composite can be used for the imaging of adenosine-5'-triphosphate (ATP) and guanosine-5'-triphosphate (GTP) in living cells as discussed by Wang et al. [87]. Liu et al. have reported the physisorption of anticancer drug SN38 and doxorubicin (DOX) onto graphene oxide nanosheet [88]. The present study may be useful to comprehend the method of releasing such drug molecules after interacting with a cellular membrane.

5. Conclusions

This article presents the structural insights into the complex of zwitterionic lipid membranes and graphene oxide (GO). In lipid multilayer systems, the complex shows coexistence of two lamellar phases; one rich in GO flakes around in the hydrocarbon region (GO-rich) while the other has the GO flakes adsorbed on the head group region (GO-poor). The electron density profiles derived from the XRR data have quantified the structural changes in the membrane revealing the thicker membrane in GO-rich phase compared to the GO-poor phase. However, the GO-poor phase exhibits a thicker head group region than the GO-rich one. The grazing incidence x-ray diffraction data have unveiled the in-plane structural re-organization of the lipid chains in the presence of the GO-flakes. While the GO-rich phase suggests a complete randomized chain configuration, there is a transition of the chain tilt in GO-poor phase from next nearest neighbor (NNN) to a nearest neighbor (NN) and then to a zero tilt in the chain. This has been observed as a function of increasing concentration of GO in the complex. These results provide a long-awaited description of organization of GO molecules in the lipid membrane which may extend the potential applications of GO-lipid complexes from bioelectronics to therapeutic molecular delivery into the cell.

Associated content

Supporting Information Available: Synthesis and characterization of GO nanoflakes (Figure S1); X-ray reflectivity from lipid multilayers in presence of GO flakes (Figure S2); *d-spacings* of GO-rich and GO-poor multilayers (Table S1); Phasing diagram of the GO-lipid complex multilayers (Figure S3) and these materials are available free of charge *via* the Internet at (*website*)

Author Contributions

P. M. performed experiments, analysed the data and wrote the initial draft of the article. G. B. performed initial experiments and contributed to improve the article. A. B. helped in performing synchrotron experiment, data extraction and analysis. S. S. R. has provided intellectual guidance and improved the article. S. K. G. was the principle investigator of the project who designed the project, performed synchrotron experiment, provided intellectual and technical guidance and finalized the article.

Acknowledgement

We thank the Science & Engineering Research Board (SERB), Department of Science and Technology (DST), India for funding the project (File no. EMR/2016/006221). We acknowledge DST for financial support and Saha Institute of Nuclear Physics, India for facilitating the experiments at the Indian Beamline, Photon Factory, KEK, Japan. We would like to thank Prof. Tim Salditt and his group for MATLAB tool used in analysing the diffraction data. P. Mandal thanks Shiv Nadar University for the research fellowship.

Table 1: Parameters corresponding the Gaussians fitted to the electron density profile of lipid multilayers in presence of different wt. % of graphene oxide (GO). Parameters of *Head 1*, *Head 2*, *Head 3*, *Head 4* and *Chain 1*, *Chain 2* are related to the Gaussians fitted to the head group and chain regions of the EDP. The GO-poor and GO-rich phases are fitted with five and six Gaussians, respectively.

Sample	DPPC (Baseline: -0.29±0.01)		DPPC/5% GO				DPPC/15% GO			
			GO poor phase (Baseline: -0.90)		GO rich phase (Baseline: -0.70)		GO poor phase (Baseline: -0.85)		GO rich phase (Baseline: -0.70)	
Gaussians	FWHM (Å) σ_n	Position (Å) Z_n	FWHM (Å) σ_n	Position (Å) Z_n	FWHM (Å) σ_n	Position (Å) Z_n	FWHM (Å) σ_n	Position (Å) Z_n	FWHM (Å) σ_n	Position (Å) Z_n
Head 1	6.51±0.02	-21.47±0.01	13.04±0.06	-22.40±0.02	10.13±0.07	-22.75±0.02	13.27±0.10	-23.00±0.02	8.42±0.07	-24.38±0.03
Head 2	4.33±0.10	-6.49±0.06	4.86±0.37	-6.62±0.25	4.42±0.22	-11.14±0.11	7.16±0.61	-8.41±0.23	4.72±0.12	-11.06±0.06
Chain 1	5.40±0.06	0	5.30±0.32	0	5.19±0.35	-4.24±0.11	5.65±0.27	0	4.99±0.35	-3.75±0.11
Chain 2	-	-	-	-	5.21±0.35	4.24±0.11	-	-	5.00±0.35	3.75±0.11
Head 3	4.33±0.10	6.49±0.06	4.91±0.38	6.63±0.26	4.45±0.23	11.15±0.11	7.20±0.62	8.43±0.23	4.72±0.12	11.07±0.06
Head 4	6.51±0.02	21.47±0.01	12.99±0.06	22.38±0.02	10.07±0.07	22.73±0.02	13.25±0.11	23.00±0.02	8.40±0.07	24.38±0.03

Table 2: Structural parameters of organization of lipid molecules obtained from the in-plane Bragg peaks (q_{xy} Vs *Intensity*) and out-of-plane Bragg rods (q_z Vs *Intensity*) under grazing incidence diffraction experiments on lipid multilayers. The d -spacings are given by d_{11} and d_{02} . The lattice parameters of the rectangular unit cell are given by a and b . L_{11} and L_{02} are the correlation lengths in the direction of q_{xy}^{11} and q_{xy}^{02} , and τ is the tilt angle of the acyl chains.

Sample	d_{11} (Å)	d_{02} (Å)	a (Å)	b (Å)	L_{11}	L_{02}	τ (°)
DPPC	5.09±0.01	4.78±0.01	6.02±0.01	9.54±0.02	119.50±10.20	138.70±16.90	25.80±0.01
DPPC/5% GO	5.07±0.10	4.82±0.02	5.96±0.40	9.64±0.07	39.10±11.00	55.80±6.10	10.90±0.02
DPPC/15% GO	5.01±0.35	4.82±0.05	5.86±0.36	9.64±0.23	32.90±12.50	52.40±22.20	-

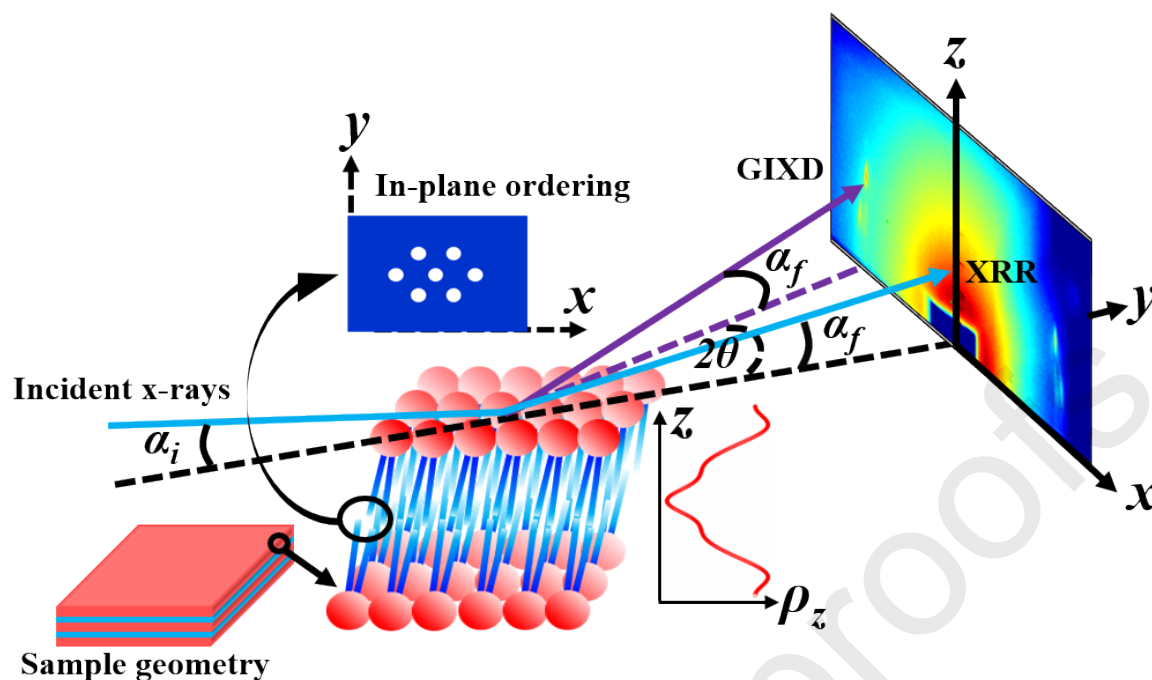


Figure 1: Schematic diagram of the x-ray scattering study employed on the lipid multilayer samples formed on a Si-substrate. In x-ray reflectivity study, the scattered intensity was collected as a function of q_z component of the wave vector transfer with the specular condition of angle of incidence (θ_i) equals to angle of reflection (θ_f). It provides the structure of the layer along the substrate normal (z -axis). In grazing incidence x-ray diffraction experiment (GIXD) the Bragg diffraction pattern was collected at a fixed angle of incidence (θ_i). This pattern could be generated from any in-plane (x - y plane) organization of lipid molecules forming a two-dimensional crystalline structure.

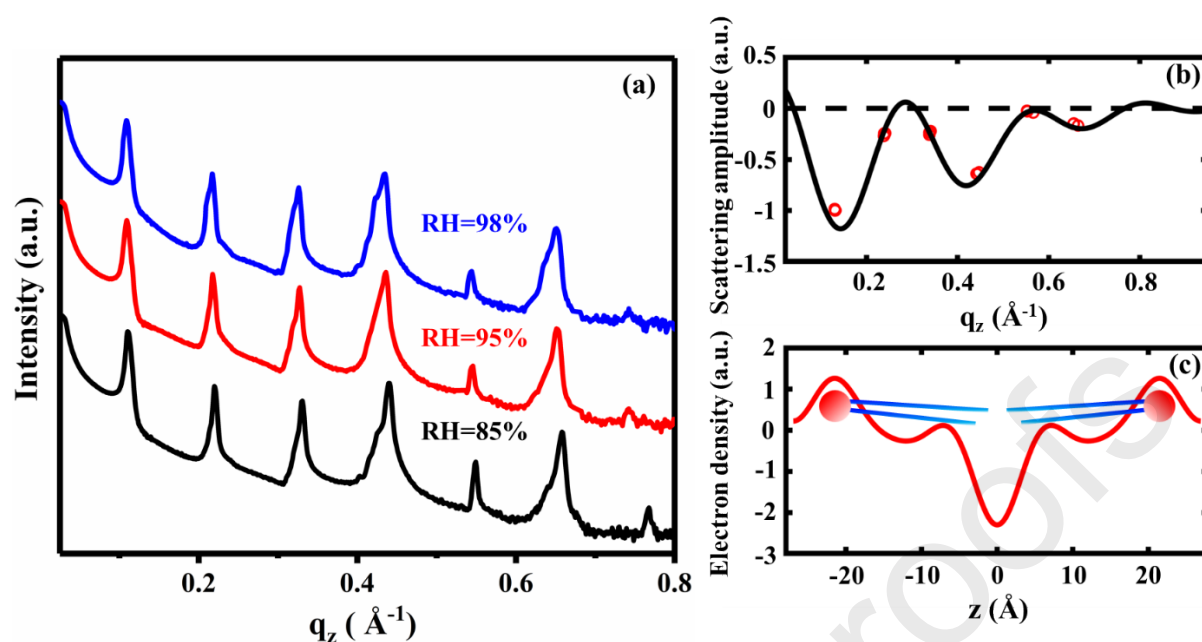


Figure 2: (a) X-ray reflectivity (*XRR*) data from a stack of DPPC lipid bilayers collected at different relative humidity (RH). The equidistant Bragg peaks are obtained from the one-dimensional crystalline arrangement of bilayers along the substrate normal (*z*-axis in Figure 1). (b) Phasing diagram obtained from data given in (a) explaining the swelling method. The solid line represents the continuous form factor while the circles are the form factor amplitudes. (c) Electron density profile (EDP) of pure DPPC multilayer obtained using swelling method (see text). The schematic of lipid molecule in the EDP describes the respective region of the EDP of a bilayer.

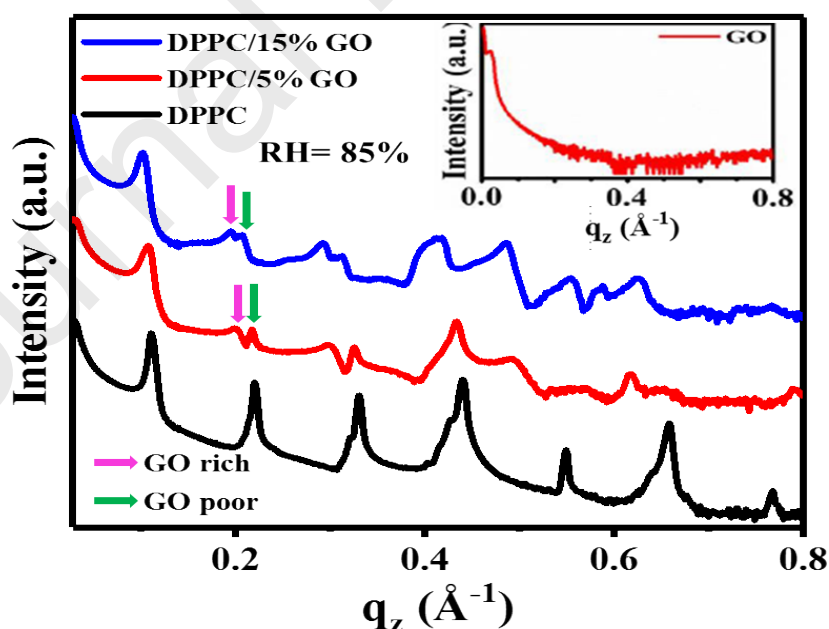


Figure 3: X-ray reflectivity pattern of DPPC multilayer with different weight percent of added GO obtained at relative humidity of 85% using a synchrotron x-ray source. The data at RH 95% and 98% are shown in Figure S2. *Inset:* X-ray reflectivity pattern of GO flakes deposited on Si substrate by drop casting.

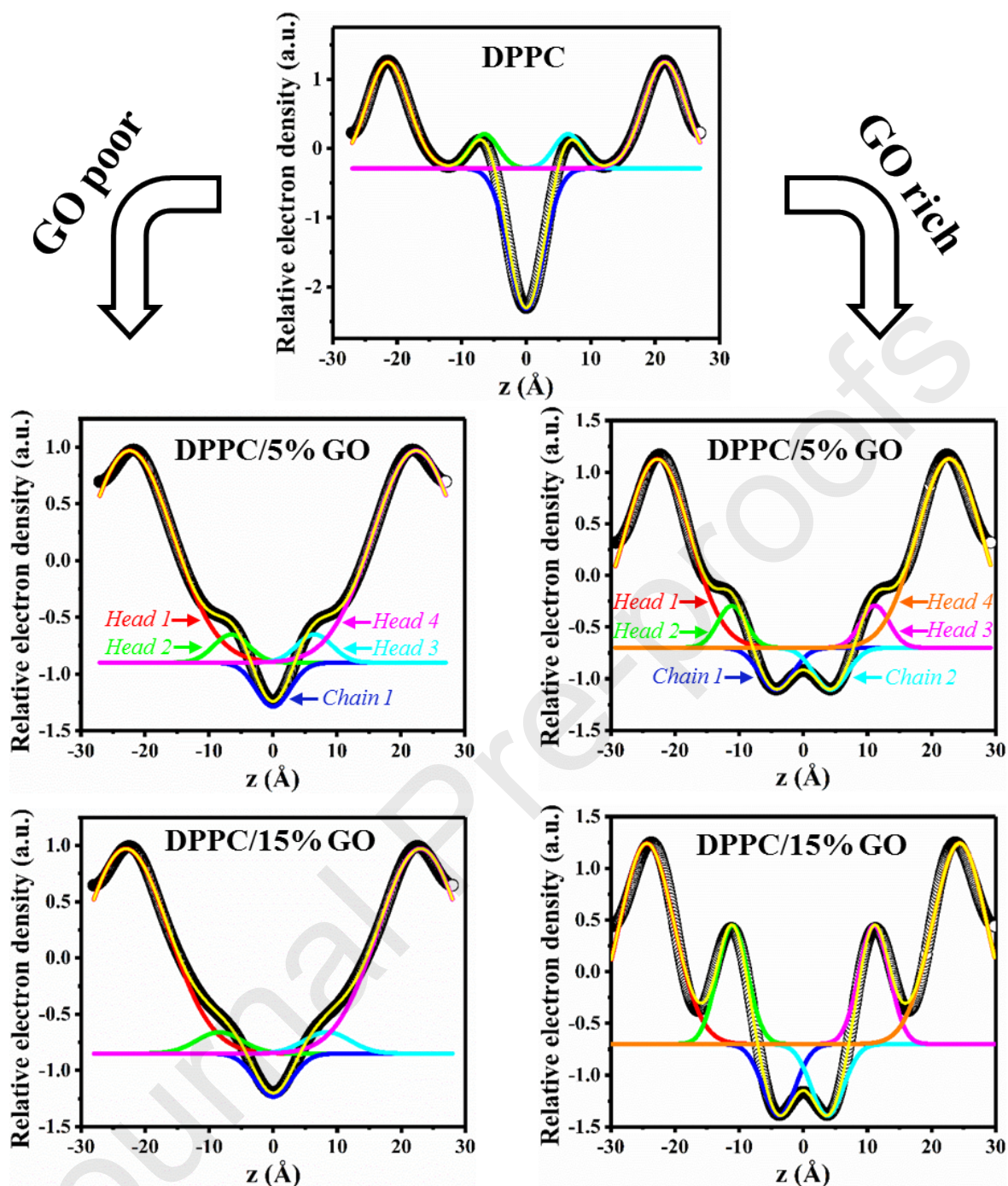


Figure 4: Electron density profiles (EDPs) of lipid bilayers formed by DPPC molecules in the presence of different wt. % of graphene oxide (GO). The EDPs are fitted with five and six Gaussians for GO-poor and GO-rich phases, respectively. The black curve in each figure is the EDP obtained from the swelling method (see text) and the yellow curve is the cumulative fit considering all the Gaussians. While GO-poor phase shows higher effects in the lipid head group region, the GO-rich phase exhibits stronger effects in the hydrocarbon chain region.

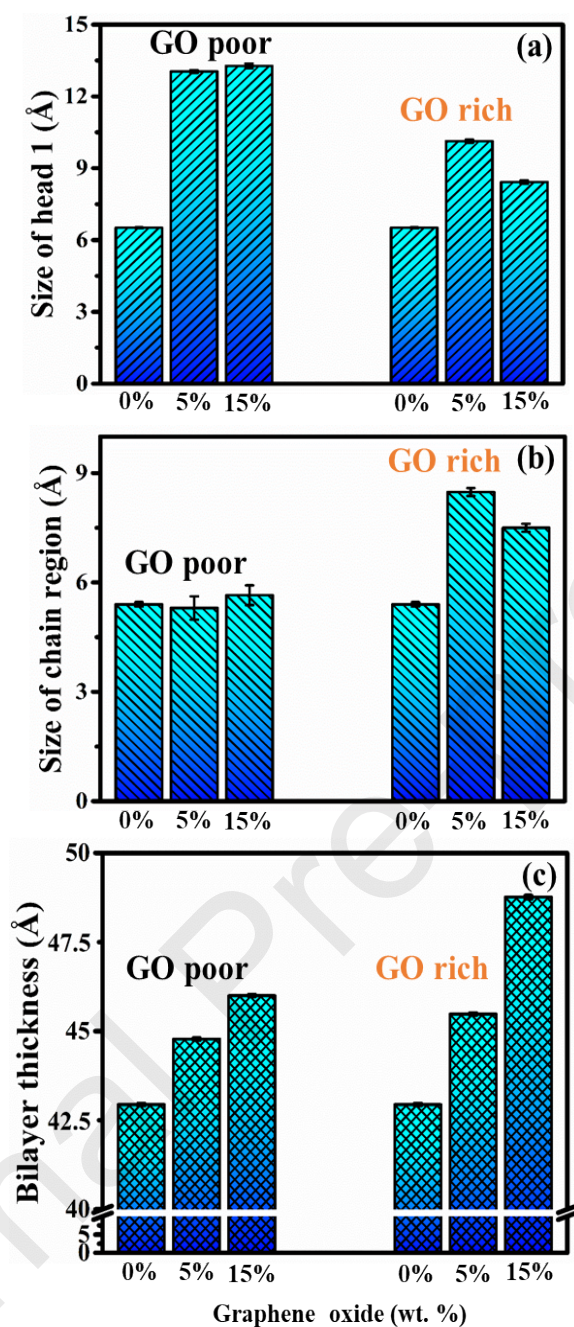


Figure 5: Structural parameters of a lipid bilayer obtained by fitting multiple Gaussians to the electron density profile (EDP) of the bilayer. (a) The full width half maxima (FWHM) of the head group region of the bilayer (denoted as size of *head 1*). (b) The size of hydrophobic chain region. (c) Bilayer thickness obtained from the positions of extreme two Gaussians positioned symmetrically on either side of the chain. In the presence of graphene oxide (GO), there is pronounced change in the head group region in GO-poor phase while it has more effect in the chain region in GO-rich phase. The GO-rich phase is thicker than the GO-poor phase.

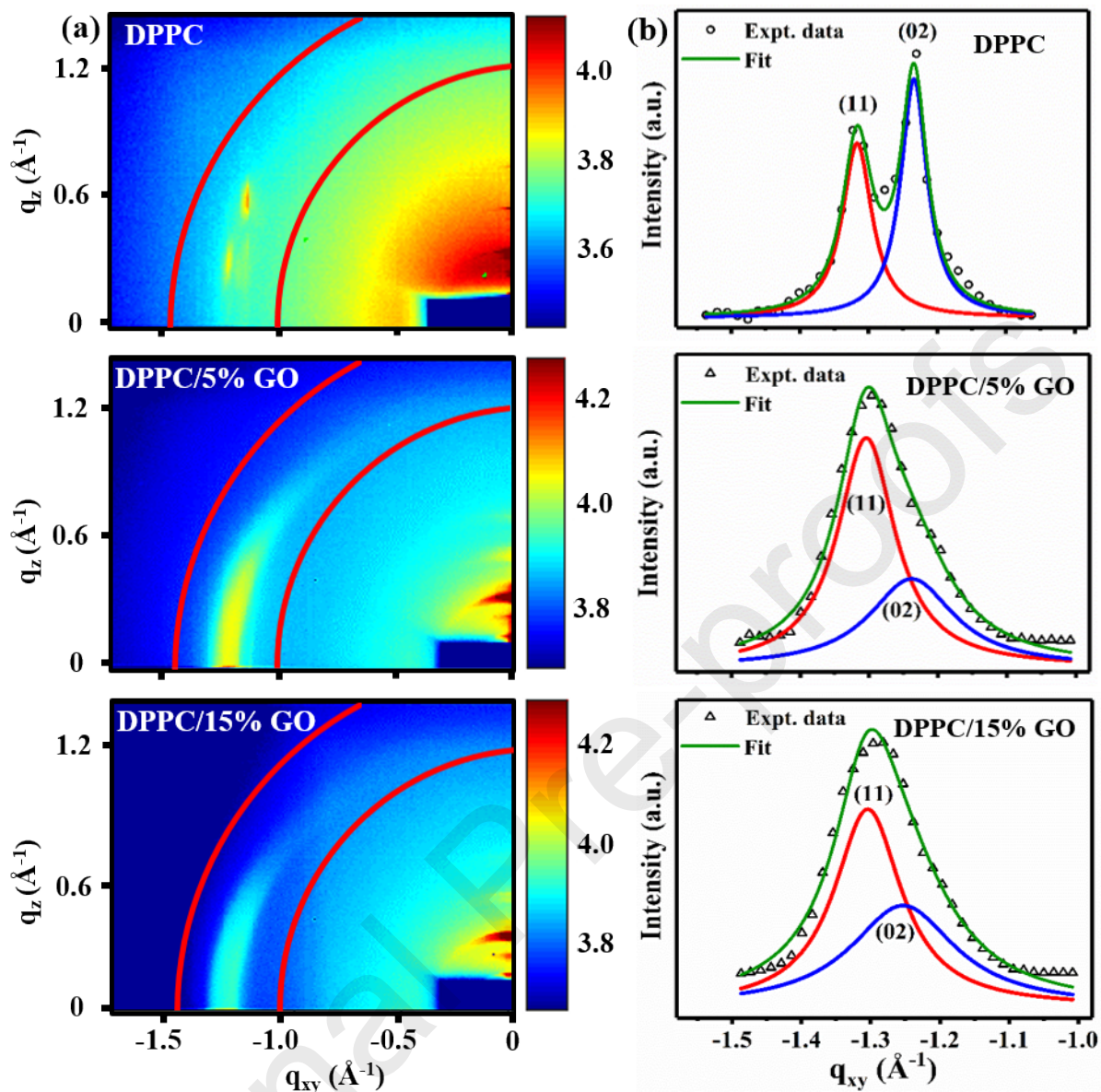


Figure 6: GIXD profile of pure DPPC and DPPC with added graphene oxide (GO) in lipid multilayers. (a) Patterns collected on a 2D detector exhibiting q_{xy} and the q_z components of wave vector transfer and (b) Bragg peaks originated from the in-plane 2D crystalline structure of lipid chains. The symbols represent the experimental data and solid lines are the Lorentzian function fits. The marked region in (a) are plotted in (b).

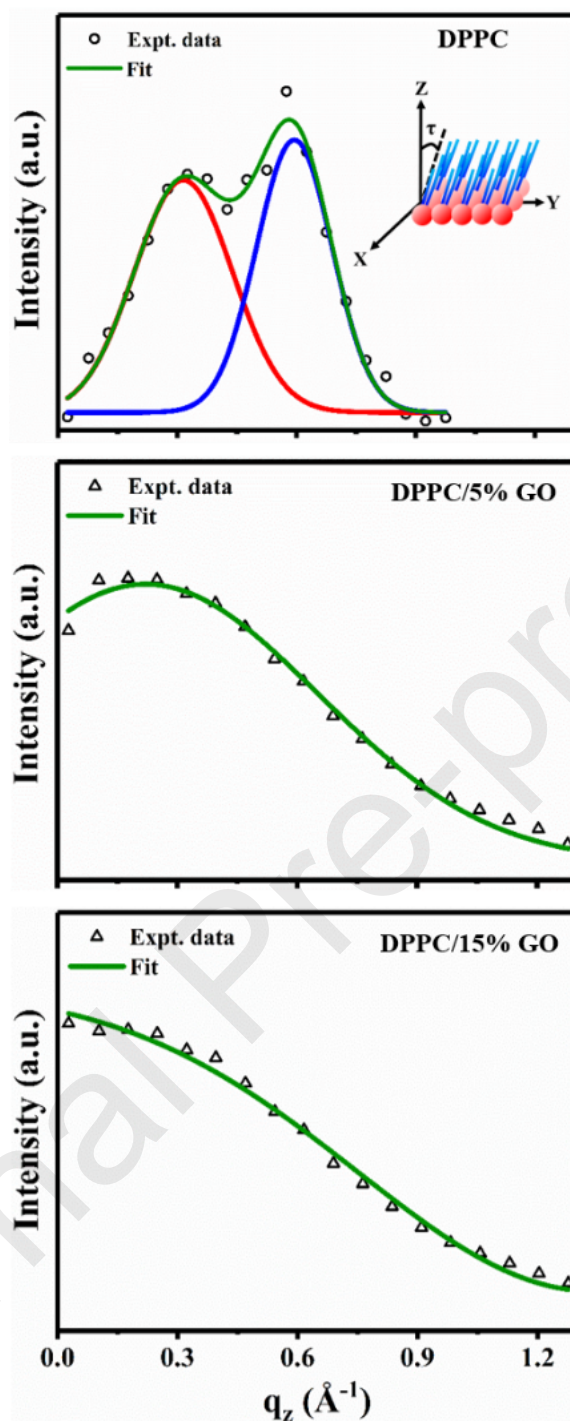


Figure 7: The intensity of Bragg rods plotted as a function of q_z for DPPC lipid multilayers with added graphene oxide (GO) in the layer. The peaks obtained at non-zero q_z suggest a tilt in the lipid chains. *Inset (top panel):* Schematic of lipid chain tilt with respect to the membrane normal.

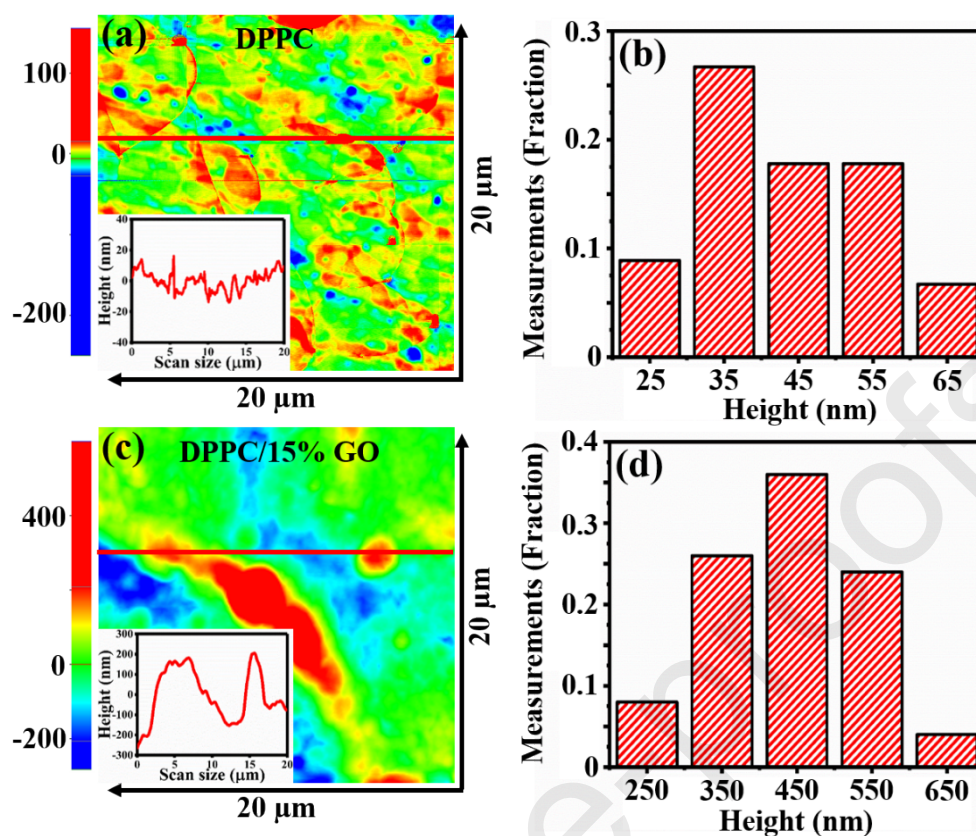


Figure 8: (a) AFM images of lipid multilayer sample of pure DPPC lipids showing a line cut in the inset and (b) distribution of the height of the line cuts obtained from different sets of samples at independent scan areas. (c) The image of a DPPC multilayer sample in the presence of 15% (w/w) graphene oxide (GO) and (d) respective distribution of height of the line cuts.

References

- [1] K.S. Novoselov, A. Geim, The rise of graphene, *Nat. Mater* 6(3) (2007) 183-191.
- [2] H. Huang, H. Shi, P. Das, J. Qin, Y. Li, X. Wang, F. Su, P. Wen, S. Li, P. Lu, *The Chemistry and Promising Applications of Graphene and Porous Graphene Materials*, *Advanced Functional Materials* (2020).
- [3] C. Peng, W. Hu, Y. Zhou, C. Fan, Q. Huang, Intracellular imaging with a graphene-based fluorescent probe, *Small* 6(15) (2010) 1686-1692.
- [4] Y. Wang, S.J. Zhen, Y. Zhang, Y.F. Li, C.Z. Huang, Facile fabrication of metal nanoparticle/graphene oxide hybrids: a new strategy to directly illuminate graphene for optical imaging, *The Journal of Physical Chemistry C* 115(26) (2011) 12815-12821.
- [5] Y. Wei, F. Zhou, D. Zhang, Q. Chen, D. Xing, A graphene oxide based smart drug delivery system for tumor mitochondria-targeting photodynamic therapy, *Nanoscale* 8(6) (2016) 3530-3538.
- [6] S. Alwarappan, A. Erdem, C. Liu, C.-Z. Li, Probing the electrochemical properties of graphene nanosheets for biosensing applications, *The Journal of Physical Chemistry C* 113(20) (2009) 8853-8857.
- [7] S. Liu, T.H. Zeng, M. Hofmann, E. Burcombe, J. Wei, R. Jiang, J. Kong, Y. Chen, Antibacterial activity of graphite, graphite oxide, graphene oxide, and reduced graphene oxide: membrane and oxidative stress, *ACS nano* 5(9) (2011) 6971-6980.
- [8] H. Watson, Biological membranes, *Essays in biochemistry* 59 (2015) 43-69.
- [9] A.V. Titov, P. Král, R. Pearson, Sandwiched graphene– membrane superstructures, *ACS nano* 4(1) (2010) 229-234.
- [10] N. Willems, A. Urtizberea, A.F. Verre, M. Iliut, M. Lelimosin, M. Hirtz, A. Vijayaraghavan, M.S. Sansom, Biomimetic phospholipid membrane organization on graphene and graphene oxide surfaces: A molecular dynamics simulation study, *ACS nano* 11(2) (2017) 1613-1625.
- [11] A.B. Seabra, A.J. Paula, R. de Lima, O.L. Alves, N. Durán, Nanotoxicity of graphene and graphene oxide, *Chemical research in toxicology* 27(2) (2014) 159-168.
- [12] Y. Chang, S.-T. Yang, J.-H. Liu, E. Dong, Y. Wang, A. Cao, Y. Liu, H. Wang, In vitro toxicity evaluation of graphene oxide on A549 cells, *Toxicology letters* 200(3) (2011) 201-210.
- [13] K.-H. Liao, Y.-S. Lin, C.W. Macosko, C.L. Haynes, Cytotoxicity of graphene oxide and graphene in human erythrocytes and skin fibroblasts, *ACS applied materials & interfaces* 3(7) (2011) 2607-2615.
- [14] X. Liu, K.L. Chen, Interactions of graphene oxide with model cell membranes: Probing nanoparticle attachment and lipid bilayer disruption, *Langmuir* 31(44) (2015) 12076-12086.
- [15] J. Chen, G. Zhou, L. Chen, Y. Wang, X. Wang, S. Zeng, Interaction of graphene and its oxide with lipid membrane: a molecular dynamics simulation study, *The Journal of Physical Chemistry C* 120(11) (2016) 6225-6231.
- [16] R. Frost, G.E. Jönsson, D. Chakarov, S. Svedhem, B. Kasemo, Graphene oxide and lipid membranes: interactions and nanocomposite structures, *Nano letters* 12(7) (2012) 3356-3362.

- [17] S. Li, A.J. Stein, A. Kruger, R.M. Leblanc, Head groups of lipids govern the interaction and orientation between graphene oxide and lipids, *The Journal of Physical Chemistry C* 117(31) (2013) 16150-16158.
- [18] A.C.F. Ip, B. Liu, P.J.J. Huang, J. Liu, Oxidation Level-Dependent Zwitterionic Liposome Adsorption and Rupture by Graphene-based Materials and Light-Induced Content Release, *Small* 9(7) (2013) 1030-1035.
- [19] L. Wu, L. Zeng, X. Jiang, Revealing the nature of interaction between graphene oxide and lipid membrane by surface-enhanced infrared absorption spectroscopy, *Journal of the American Chemical Society* 137(32) (2015) 10052-10055.
- [20] Y. Tu, M. Lv, P. Xiu, T. Huynh, M. Zhang, M. Castelli, Z. Liu, Q. Huang, C. Fan, H. Fang, Destructive extraction of phospholipids from *Escherichia coli* membranes by graphene nanosheets, *Nature nanotechnology* 8(8) (2013) 594.
- [21] W. Meng, E. Gall, F. Ke, Z. Zeng, B. Kopchick, R. Timsina, X. Qiu, Structure and interaction of graphene oxide–cetyltrimethylammonium bromide complexation, *The Journal of Physical Chemistry C* 119(36) (2015) 21135-21140.
- [22] A.M. Dimiev, J.M. Tour, Mechanism of graphene oxide formation, *ACS nano* 8(3) (2014) 3060-3068.
- [23] Y. Ma, S.K. Ghosh, D.A. DiLena, S. Bera, L.B. Lurio, A.N. Parikh, S.K. Sinha, Cholesterol partition and condensing effect in phase-separated ternary mixture lipid multilayers, *Biophysical journal* 110(6) (2016) 1355-1366.
- [24] A. Wexler, S. Hasegawa, Relative Humidity-Temperature Relationships of Some Saturated Salt Solutions in the Temperature Range 0 to 50 C1, *NBS Special Publication* (300-308) (1972) 277.
- [25] C. Lee, P. Slade, Miscarriage as a traumatic event: a review of the literature and new implications for intervention, *Journal of psychosomatic research* 40(3) (1996) 235-244.
- [26] Z. Jiang, GIXSGUI: a MATLAB toolbox for grazing-incidence X-ray scattering data visualization and reduction, and indexing of buried three-dimensional periodic nanostructured films, *Journal of Applied Crystallography* 48(3) (2015) 917-926.
- [27] G. Pabst, N. Kučerka, M.-P. Nieh, M. Rheinstädter, J. Katsaras, Applications of neutron and X-ray scattering to the study of biologically relevant model membranes, *Chemistry and Physics of Lipids* 163(6) (2010) 460-479.
- [28] J. Als-Nielsen, D. Jacquemain, K. Kjaer, F. Leveiller, M. Lahav, L. Leiserowitz, Principles and applications of grazing incidence x-ray and neutron scattering from ordered molecular monolayers at the air-water interface, *Physics Reports* 246(5) (1994) 254.
- [29] G. King, C. Worthington, Analytic continuation as a method of phase determination, *Physics Letters A* 35(4) (1971) 259-260.
- [30] S. Tristram-Nagle, H.I. Petrache, J.F. Nagle, Structure and interactions of fully hydrated dioleoylphosphatidylcholine bilayers, *Biophysical journal* 75(2) (1998) 917-925.
- [31] K. Hristova, S. White, Determination of the hydrocarbon core structure of fluid DOPC bilayers by x-ray diffraction using specific bromination of the double-bonds: effect of hydration, *Biophys. J* 74 (1998) 2419-2433.
- [32] A.E. Blaurock, Structure of the nerve myelin membrane: proof of the low-resolution profile, *Journal of molecular biology* 56(1) (1971) 35-52.

- [33] J.F. Nagle, S. Tristram-Nagle, Structure of lipid bilayers, *Biochimica et Biophysica Acta (BBA)-Reviews on Biomembranes* 1469(3) (2000) 159-195.
- [34] S. Costigan, P. Booth, R. Templer, Estimations of lipid bilayer geometry in fluid lamellar phases, *Biochimica et Biophysica Acta (BBA)-Biomembranes* 1468(1-2) (2000) 41-54.
- [35] M. Vogel, C. Münster, W. Fenzl, D. Thiaudiere, T. Salditt, Fully hydrated and highly oriented membranes: an experimental setup amenable to specular and diffuse X-ray scattering, *Physica B: Condensed Matter* 283(1-3) (2000) 32-36.
- [36] U. Mennicke, T. Salditt, Preparation of solid-supported lipid bilayers by spin-coating, *Langmuir* 18(21) (2002) 8172-8177.
- [37] V. Raghunathan, J. Katsaras, Structure of the $l c'$ phase in a hydrated lipid multilamellar system, *Physical review letters* 74(22) (1995) 4456.
- [38] S. Karmakar, V. Raghunathan, Structure of phospholipid-cholesterol membranes: An x-ray diffraction study, *Physical Review E* 71(6) (2005) 061924.
- [39] G. Pabst, J. Katsaras, V.A. Raghunathan, M. Rappolt, Structure and interactions in the anomalous swelling regime of phospholipid bilayers, *Langmuir* 19(5) (2003) 1716-1722.
- [40] S.K. Ghosh, S. Aeffner, T. Salditt, Effect of PIP2 on Bilayer Structure and Phase Behavior of DOPC: An X-ray Scattering Study, *ChemPhysChem* 12(14) (2011) 2633-2640.
- [41] R.J. Alsop, R.M. Schober, M.C. Rheinstädter, Swelling of phospholipid membranes by divalent metal ions depends on the location of the ions in the bilayers, *Soft Matter* 12(32) (2016) 6737-6748.
- [42] F. Chen, W. Hung, H.W. Huang, Critical swelling of phospholipid bilayers, *Physical review letters* 79(20) (1997) 4026.
- [43] T.J. McIntosh, A.D. Magid, S.A. Simon, Cholesterol modifies the short-range repulsive interactions between phosphatidylcholine membranes, *Biochemistry* 28(1) (1989) 17-25.
- [44] C. Münster, J. Lu, B. Bechinger, T. Salditt, Grazing incidence X-ray diffraction of highly aligned phospholipid membranes containing the antimicrobial peptide magainin 2, *European Biophysics Journal* 28(8) (2000) 683-688.
- [45] Y. Wu, K. He, S.J. Ludtke, H.W. Huang, X-ray diffraction study of lipid bilayer membranes interacting with amphiphilic helical peptides: diphytanoyl phosphatidylcholine with alamethicin at low concentrations, *Biophysical journal* 68(6) (1995) 2361-2369.
- [46] A. Spaar, C. Münster, T. Salditt, Conformation of peptides in lipid membranes studied by x-ray grazing incidence scattering, *Biophysical journal* 87(1) (2004) 396-407.
- [47] K. Kumar, M. Chavarha, R.W. Loney, T.M. Weiss, S.B. Ranavavare, S.B. Hall, The $L\gamma$ Phase of Pulmonary Surfactant, *Langmuir* 34(22) (2018) 6601-6611.
- [48] A. Küsel, Z. Khattari, P.E. Schneggenburger, A. Banerjee, T. Salditt, U. Diederichsen, Conformation and Interaction of ad, l-Alternating Peptide with a Bilayer Membrane: X-ray Reflectivity, CD, and FTIR Spectroscopy, *ChemPhysChem* 8(16) (2007) 2336-2343.
- [49] S. Gosh, B. Salgin, D. Pontoni, T. Reusch, P. Keil, D. Vogel, M. Rohwerder, H. Reichert, T. Salditt, Structure and Volta Potential of Lipid Multilayers: Effect of X-ray Radiation, *Langmuir* 29 (2013) 815-824.
- [50] C.-C. Lee, Y. Sun, S. Qian, H.W. Huang, Transmembrane pores formed by human antimicrobial peptide LL-37, *Biophysical journal* 100(7) (2011) 1688-1696.

- [51] G.I. King, S.H. White, Determining bilayer hydrocarbon thickness from neutron diffraction measurements using strip-function models, *Biophysical journal* 49(5) (1986) 1047-1054.
- [52] G. Bhattacharya, R. Giri, H. Saxena, V. Agrawal, A. Gupta, M. Mukhopadhyay, S. Ghosh, X-ray reflectivity study of the interaction of an imidazolium-based ionic liquid with a soft supported lipid membrane, *Langmuir* 33(5) (2017) 1295-1304.
- [53] M. Wiener, R. Suter, J. Nagle, Structure of the fully hydrated gel phase of dipalmitoylphosphatidylcholine, *Biophysical journal* 55(2) (1989) 315-325.
- [54] H. Jing, D. Hong, B. Kwak, D. Choi, K. Shin, C.-J. Yu, J. Kim, D. Noh, Y. Seo, X-ray reflectivity study on the structure and phase stability of mixed phospholipid multilayers, *Langmuir* 25(7) (2009) 4198-4202.
- [55] E. Drolle, N. Kučerka, M. Hoopes, Y. Choi, J. Katsaras, M. Karttunen, Z. Leonenko, Effect of melatonin and cholesterol on the structure of DOPC and DPPC membranes, *Biochimica et Biophysica Acta (BBA)-Biomembranes* 1828(9) (2013) 2247-2254.
- [56] J.F. Nagle, P. Cognet, F.G. Dupuy, S. Tristram-Nagle, Structure of gel phase DPPC determined by X-ray diffraction, *Chemistry and physics of lipids* 218 (2019) 168-177.
- [57] K. Jørgensen, J.H. Ipsen, O.G. Mouritsen, D. Bennett, M.J. Zuckermann, A general model for the interaction of foreign molecules with lipid membranes: drugs and anaesthetics, *Biochimica et Biophysica Acta (BBA)-Biomembranes* 1062(2) (1991) 227-238.
- [58] K. Kjaer, Some simple ideas on x-ray reflection and grazing incidence diffraction from thin surfactant films, *Physica B* 198 (1994) 100-109.
- [59] T.R. Jensen, K. Kjær, Structural properties and interactions of thin films at the air-liquid interface explored by synchrotron X-ray scattering, *Novel methods to study interfacial layers* 11 (2001) 2054.
- [60] V.M. Kaganer, H. Möhwald, P. Dutta, Structure and phase transitions in Langmuir monolayers, *Reviews of Modern Physics* 71(3) (1999) 779.
- [61] S. Karmakar, V. Raghunathan, S. Mayor, Phase behaviour of dipalmitoyl phosphatidylcholine (DPPC)-cholesterol membranes, *Journal of Physics: Condensed Matter* 17(14) (2005) S1177.
- [62] K. Hąc-Wydro, M. Flasiński, M. Broniatowski, P. Dynarowicz-Łątka, J. Majewski, Properties of β -sitostanol/DPPC monolayers studied with Grazing Incidence X-ray Diffraction (GIXD) and Brewster Angle Microscopy, *Journal of colloid and interface science* 364(1) (2011) 133-139.
- [63] P. Scherrer, Bestimmung der inneren Struktur und der Größe von Kolloidteilchen mittels Röntgenstrahlen, *Kolloidchemie Ein Lehrbuch*, Springer 1912, pp. 387-409.
- [64] A. Patterson, The Scherrer formula for X-ray particle size determination, *Physical review* 56(10) (1939) 978.
- [65] S. Tristram-Nagle, Y. Liu, J. Legleiter, J.F. Nagle, Structure of gel phase DMPC determined by X-ray diffraction, *Biophysical journal* 83(6) (2002) 3324-3335.
- [66] S. Tristram-Nagle, R. Zhang, R. Suter, C. Worthington, W. Sun, J. Nagle, Measurement of chain tilt angle in fully hydrated bilayers of gel phase lecithins, *Biophysical journal* 64(4) (1993) 1097-1109.

- [67] W.-J. Sun, R. Suter, M. Knewton, C. Worthington, S. Tristram-Nagle, R. Zhang, J. Nagle, Order and disorder in fully hydrated unoriented bilayers of gel-phase dipalmitoylphosphatidylcholine, *Physical Review E* 49(5) (1994) 4665.
- [68] V. Raghunathan, J. Katsaras, L $\beta' \rightarrow$ L c' phase transition in phosphatidylcholine lipid bilayers: A disorder-order transition in two dimensions, *Physical Review E* 54(4) (1996) 4446.
- [69] E. Watkins, C. Miller, D. Mulder, T. Kuhl, J. Majewski, Structure and orientational texture of self-organizing lipid bilayers, *Physical review letters* 102(23) (2009) 238101.
- [70] K. Akabori, J.F. Nagle, Structure of the DMPC lipid bilayer ripple phase, *Soft matter* 11(5) (2015) 918-926.
- [71] D. Marsh, Lateral order in gel, subgel and crystalline phases of lipid membranes: Wide-angle X-ray scattering, *Chemistry and physics of lipids* 165(1) (2012) 59-76.
- [72] S.K. Ghosh, S. Castorph, O. Kononov, T. Salditt, R. Jahn, M. Holt, Measuring Ca^{2+} -induced structural changes in lipid monolayers: implications for synaptic vesicle exocytosis, *Biophysical journal* 102(6) (2012) 1394-1402.
- [73] J. Israelachvili, *Intermolecular and Surface Forces Preface to the Third Edition*, Intermolecular and Surface Forces, 3rd ed.; Academic Press: Burlington, MA, USA (2011).
- [74] T. Salditt, K. Komorowski, K. Frank, 2 X-ray structure analysis of lipid membrane systems: solid-supported bilayers, bilayer stacks, and vesicles, *Characterization of Biological Membranes: Structure and Dynamics* (2019) 43.
- [75] S. Karmakar, V. Raghunathan, Cholesterol-induced modulated phase in phospholipid membranes, *Physical review letters* 91(9) (2003) 098102.
- [76] S.L. Veatch, S.L. Keller, Separation of liquid phases in giant vesicles of ternary mixtures of phospholipids and cholesterol, *Biophysical journal* 85(5) (2003) 3074-3083.
- [77] M.C. Blosser, J.B. Starr, C.W. Turtle, J. Ashcraft, S.L. Keller, Minimal effect of lipid charge on membrane miscibility phase behavior in three ternary systems, *Biophysical journal* 104(12) (2013) 2629-2638.
- [78] R. Brewster, P.A. Pincus, S.A. Safran, Hybrid lipids as a biological surface-active component, *Biophysical journal* 97(4) (2009) 1087-1094.
- [79] L. Tayebi, Y. Ma, D. Vashaee, G. Chen, S.K. Sinha, A.N. Parikh, Long-range interlayer alignment of intralayer domains in stacked lipid bilayers, *Nature materials* 11(12) (2012) 1074-1080.
- [80] J.-X. Cheng, S. Pautot, D.A. Weitz, X.S. Xie, Ordering of water molecules between phospholipid bilayers visualized by coherent anti-Stokes Raman scattering microscopy, *Proceedings of the National Academy of Sciences* 100(17) (2003) 9826-9830.
- [81] S.P. Mukherjee, B. Lazzaretto, K. Hultenby, L. Newman, A.F. Rodrigues, N. Lozano, K. Kostarelos, P. Malmberg, B. Fadeel, Graphene oxide elicits membrane lipid changes and neutrophil extracellular trap formation, *Chem* 4(2) (2018) 334-358.
- [82] P.W. Fenimore, H. Frauenfelder, B. McMahan, R. Young, Bulk-solvent and hydration-shell fluctuations, similar to α - and β -fluctuations in glasses, control protein motions and functions, *Proceedings of the National Academy of Sciences* 101(40) (2004) 14408-14413.
- [83] P.-J.J. Huang, F. Wang, J. Liu, Liposome/graphene oxide interaction studied by isothermal titration calorimetry, *Langmuir* 32(10) (2016) 2458-2463.
- [84] S. Li, J. Guo, R.A. Patel, A.L. Dadlani, R.M. Leblanc, Interaction between graphene oxide and pluronic f127 at the air-water interface, *Langmuir* 29(19) (2013) 5742-5748.

- [85] E. Puigpelat, J. Ignés-Mullol, F. Sagués, R. Reigada, Interaction of Graphene Nanoparticles and Lipid Membranes Displaying Different Liquid Orderings: A Molecular Dynamics Study, *Langmuir* 35(50) (2019) 16661-16668.
- [86] N. Mohanty, V. Berry, Graphene-based single-bacterium resolution biodevice and DNA transistor: interfacing graphene derivatives with nanoscale and microscale biocomponents, *Nano letters* 8(12) (2008) 4469-4476.
- [87] Y. Wang, Z. Li, T.J. Weber, D. Hu, C.-T. Lin, J. Li, Y. Lin, In situ live cell sensing of multiple nucleotides exploiting DNA/RNA aptamers and graphene oxide nanosheets, *Analytical chemistry* 85(14) (2013) 6775-6782.
- [88] Z.R. Liu, JT; Sun, XM; Dai, HJ PEGylated nanographene oxide for delivery of water-insoluble cancer drugs, *J. Am. Chem. Soc* 130 (2008) 10876-10877.

Author Contributions

P. M. performed experiments, analysed the data and wrote the initial draft of the article. G. B. performed initial experiments and contributed to improve the article. A. B. helped in performing synchrotron experiment, data extraction and analysis. S. S. R. has provided intellectual guidance and improved the article. S. K. G. was the principle investigator of the project who designed the project, performed synchrotron experiment, provided intellectual and technical guidance and finalized the article.

Declaration of interests

The authors declare that they have no known competing financial interests or personal relationships that could have appeared to influence the work reported in this paper.

□The authors declare the following financial interests/personal relationships which may be considered as potential competing interests:

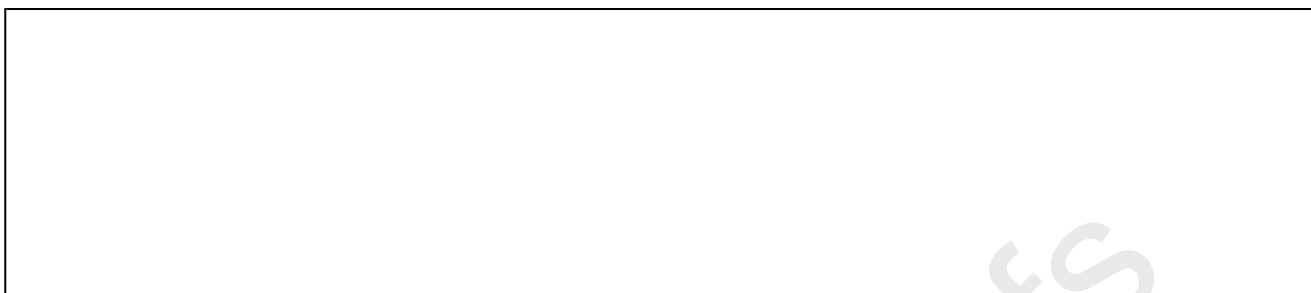
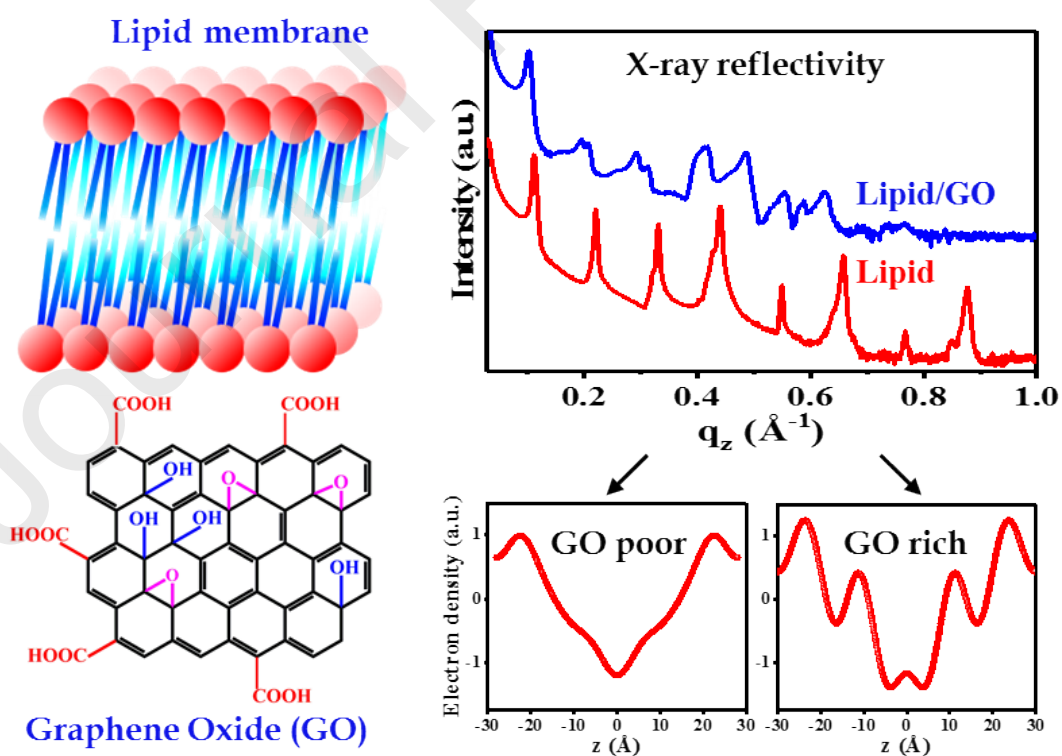


Table of content (TOC)



To,

13th October 2020

The Reviewers
Applied Surface Science

Dear Respected Reviewers,

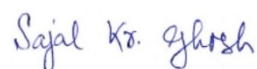
We would like to THANK YOU for reviewing our manuscript entitled “**Unravelling the Structural Changes of Phospholipid Membranes in Presence of Graphene Oxide**”. We deeply appreciate your valuable suggestions for improving the scientific content of the manuscript. Followings are the noticeable changes made in the revised manuscript,

- ⇒ The TOC has been modified for a vivid description of the content of the paper.
- ⇒ Following newly performed x-ray photoelectron spectroscopy (XPS) experiment, the atomic percentage of O₂ in the graphene oxide (GO) flakes has been mentioned in the revised manuscript, which was not there in the originally submitted manuscript.
- ⇒ A detailed discussion about the possible origin of self-assembly of the GO flakes in the membrane has been added. This would definitely be helpful to extend our present understanding of the field.
- ⇒ A new section has been included;

3. 4 Limitations and future prospects:

As the revised manuscript has presented a better understanding of the experimental data, we hope it to be suitable now for publishing in Applied Surface Science.

With best regards



(Dr. Sajal Kumar Ghosh)

Manuscript Title: Unravelling the Structural Changes of Phospholipid Membranes in Presence of Graphene Oxide

Corresponding Author: Dr. Sajal Kumar Ghosh

Mailing Address: Department of Physics, School of Natural Sciences, Shiv Nadar University, NH-91, Tehsil Dadri, G. B. Nagar, Uttar Pradesh, 201314, India

Phone Number: +91-8527695318

E-mail: sajal.ghosh@snu.edu.in

Table of content (TOC)

